tails of the resonance conditions are given in Brannen and Froelich[6] and Froelich.[3] The magnetic guide field is split into four sectors with a uniform field within the sectors, and regions of a low magnetic field between the sectors. To obtain stability of the betatron oscillations, thus achieving focusing of the beam, magnetic shields have been installed in two regions between the sectors, reducing the magnetic field in these regions. The magnetic gap within the sectors has a width of only 7 mm. The energy gain per orbit can be varied within wide limits (0.40–1.5 Mev) and synchronism obtained by adjusting the distance between the symmetrical half of the magnetic guide field. The lower limit of the range is determined by the width of the cavity and gun assembly, the upper limit by the power available and RF breakdown in the cavity. With the present arrangement this gives a lower limit of 780 kev per orbit. We have operated as low as 400 kev with the gun removed and field emission from the walls of a re-entrant cavity supplying the current. The upper limit could be as much as 1.5 Mev per orbit if power is supplied by two magnetrons. At the present time one magnetron (RK 5586) is used supplying 600 kw peak power (pulse duration 2 μsec). For electron injection, a simple Pierce gun is used giving a current of 300 ma at 20 kev. The electrons are injected into the cavity by means of small auxiliary pole pieces.

The highest currents obtained to date are 20 ma in the third orbit and 2.5 ma in the final (eighth) orbit with an energy of 6.2 Mev in the eighth orbit. The high current dropoff from third to eighth orbit is due to the fact, that, because of beam loading, the accelerator does not operate in perfect synchronism. With an RF source giving slightly more power than the presently used magnetron, the current in the final orbit should exceed 10 ma. This assumption is substantiated by the fact that at lower currents ($<$1ma) the current drops off from third to eighth orbit only by a factor of 1.5. The bunching behavior of the racetrack microtron is theoretically similar to that of a conventional microtron, *i.e.*, with an optimum bunching to be expected in the third orbit. In an actual submillimeter wave generator a three-orbit machine might therefore be used, giving a fairly compact design, and such a device is being designed on the basis of the present machine. As far as the extraction of electromagnetic radiation from a bunched beam is concerned, we have not been able to use the beam of the racetrack microtron for that purpose in time for this conference. So far we have been using Cerenkov and transition radiators to extract radiation from an electron beam accelerated by a simple cavity. We plan to continue this series of experiments in the near future using the beam of the racetrack microtron.

ACKNOWLEDGMENT

The authors are grateful to their colleagues T. W. W. Stewart, V. Rutulis, V. Sells and D. Rumbold for their assistance in the construction and operation of the microtron.

[6] E. Brannen and H. Froelich, "Preliminary operation of a four-sector racetrack microtron," *J. Appl. Phys.*, vol. 32, pp. 1179–1180; June, 1961.

The Groove Guide, a Low-Loss Waveguide for Millimeter Waves*

F. J. TISCHER†, FELLOW, IEEE

Summary—A new waveguide for the low-loss transmission of millimeter waves is presented. The guide consists of two parallel conducting walls with grooves in the central region of the guide cross section. The grooves run along the guide in the direction of the wave propagation. It is shown that the waveguide, if excited in the TE-wave mode, has properties similar to those of the H guide, which contains a dielectric slab between the conducting walls in the center. The new guide is characterized by an exponential transverse decrease of the field distributions in direction from the center and by low attenuation. Theoretical considerations dealing with the field distribution and the data of the guide are presented.

* Received January 21, 1963; revised manuscript received April 8, 1963.

† Research Institute, University of Alabama, Huntsville, Ala.

INTRODUCTION

IT CAN BE SHOWN that a waveguide which consists of two parallel conducting walls has low attenuation if excited by TE waves. For this wave mode, the electric-field vector is parallel to the conducting walls. The attenuation has characteristics similar to those of the circular waveguide excited by TE_{01} waves; namely, it is low and decreases with increasing frequency.

The H-guide, which consists of two parallel conducting walls and a centrally located transverse dielectric slab running along the guide in the direction of the wave propagation, has similar low-loss properties [1, 2]. In

this guide, the direction of the field vectors and the field distributions, in the region of maximum energy transport, are equal to those in the parallel-wall guide. The main difference consists in an exponential decrease of the field intensities in the H-guide in direction from the center parallel to the walls caused by the centrally located dielectric slab. The dielectric losses yield a major contribution to the attenuation of this guide.

In a new waveguide, which basically also consists of two conducting walls facing each other, grooves in these walls located in the central region of the guide cross section and running along the guide have a similar effect as the dielectric slab in the H-guide. The grooves cause the field distribution to decrease exponentially from the center. Since no dielectrics are used in this guide, the dielectric losses are eliminated with a corresponding reduction of the attenuation. A basic theoretical consideration of this new waveguide structure is the topic of this paper.

A method of applying conformal mapping in a general theory of the groove guide, as the new waveguide may be called, is presented first. The application of this method to a rectangular cross section of the groove is considered next. Finally, a procedure for obtaining approximate values of the cutoff and guided wavelengths in the groove guide is shown.

Deformed-Wall Guide

Let us first consider generally the effect of deformations of the wall surfaces facing each other in a parallel-wall waveguide, as indicated in Fig. 1(a). The deformations have the form of grooves. In these considerations, we assume orthogonal cylindrical coordinates. The longitudinal coordinate points in the direction of wave propagation. The transverse coordinates are chosen such that the walls represent surfaces of constant magnitudes of one of the cross-sectional coordinates. We compare the field intensities for degenerate TE waves in this guide which is air-filled with those in a true parallel-wall guide as shown in Fig. 1(b). The medium between the conducting walls of this latter guide is anisotropic and nonuniform over the cross section.

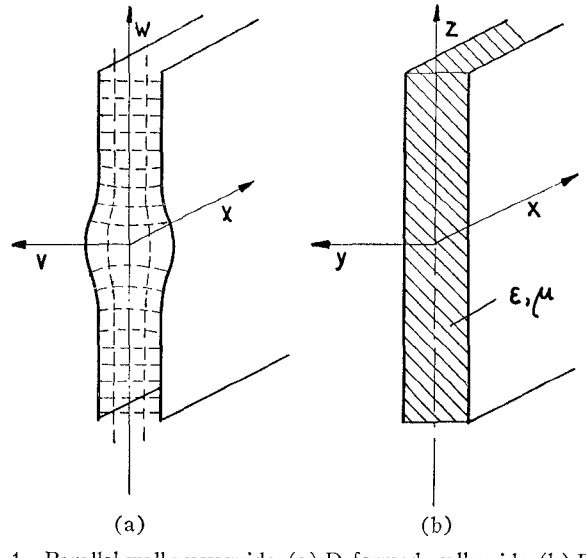

Fig. 1—Parallel-wall waveguide. (a) Deformed-wall guide. (b) Parallel-wall guide with nonuniform and anisotropic medium.

We write Maxwell's equations:

$$\nabla \times \boldsymbol{E} = -j\omega\mu H, \tag{1}$$

$$\nabla \times \boldsymbol{H} = j\omega\epsilon E, \tag{2}$$

$$\nabla \cdot \boldsymbol{D} = 0, \tag{3}$$

$$\nabla \cdot \boldsymbol{B} = 0, \tag{4}$$

where

$$\boldsymbol{B} = \mu \boldsymbol{H} = \mu_0 \mu_r \boldsymbol{H}, \tag{5}$$

$$\boldsymbol{D} = \epsilon \boldsymbol{E} = \epsilon_0 \epsilon_r \boldsymbol{E}. \tag{6}$$

Developing Maxwell's equations for the deformed-wall air-filled guide in the coordinate system for which a length element is given by

$$ds^2 = dx^2 + (hdv)^2 + (hdw)^2 \tag{7}$$

yields the following equation system:

$$\frac{\partial(hH_w)}{\partial v} - \frac{\partial(hH_v)}{\partial w} = j\omega\epsilon_0 h^2 E_x, \tag{8}$$

$$\frac{\partial H_x}{\partial w} - \frac{\partial(hH_w)}{\partial x} = j\omega\epsilon_0 h E_v, \tag{9}$$

$$\frac{\partial(hH_v)}{\partial x} - \frac{\partial H_x}{\partial v} = j\omega\epsilon_0 h E_w, \tag{10}$$

$$\frac{\partial(hE_w)}{\partial v} - \frac{\partial(hE_v)}{\partial w} = -j\omega\mu_0 h^2 H_x, \tag{11}$$

$$\frac{\partial E_x}{\partial w} - \frac{\partial(hE_w)}{\partial x} = -j\omega\mu_0 h H_v, \tag{12}$$

$$\frac{\partial(hE_v)}{\partial x} - \frac{\partial E_x}{\partial v} = -j\omega\mu_0 h H_w, \tag{13}$$

$$h^2 \frac{\partial E_x}{\partial x} + \frac{\partial(hE_v)}{\partial v} + \frac{\partial(hE_w)}{\partial w} = 0, \tag{14}$$

$$h^2 \frac{\partial H_x}{\partial x} + \frac{\partial(hH_v)}{\partial v} + \frac{\partial(hH_w)}{\partial w} = 0. \tag{15}$$

The corresponding equation system for the dielectric-filled parallel-wall guide is:

$$\frac{\partial H_z}{\partial y} - \frac{\partial H_y}{\partial z} = j\omega\epsilon_{xx} E_x, \tag{16}$$

$$\frac{\partial H_x}{\partial z} - \frac{\partial H_z}{\partial x} = j\omega\epsilon_{yy} E_y, \tag{17}$$

$$\frac{\partial H_y}{\partial x} - \frac{\partial H_x}{\partial y} = j\omega\epsilon_{zz} E_z, \tag{18}$$

$$\frac{\partial E_z}{\partial y} - \frac{\partial E_y}{\partial z} = -j\omega\mu_{xx}H_x, \tag{19}$$

$$\frac{\partial E_x}{\partial z} - \frac{\partial E_z}{\partial x} = -j\omega\mu_{yy}H_y, \tag{20}$$

$$\frac{\partial E_y}{\partial x} - \frac{\partial E_x}{\partial y} = -j\omega\mu_{zz}H_z, \tag{21}$$

$$\mu_{xx}\frac{\partial H_x}{\partial x} + \frac{\partial(\mu_{yy}H_y)}{\partial y} + \frac{\partial(\mu_{zz}H_z)}{\partial z} = 0 \tag{22}$$

$$\epsilon_{xx}\frac{\partial E_x}{\partial x} + \frac{\partial(\epsilon_{yy}E_y)}{\partial y} + \frac{\partial(\epsilon_{zz}E_z)}{\partial z} = 0 \tag{23}$$

where $\epsilon, \mu_{n,m} = 0$ for $n, m = x, y, z$ and $n \neq m$.

Comparison of these two equation systems shows interesting relationships. If we introduce the following identities, we can transform one system into the other one. The identities are

$$\begin{aligned} H_x &= H_x, & E_x &= E_x, \\ hH_v &= H_y, & hE_v &= E_y, \\ hH_w &= H_z, & hE_w &= E_z, \\ \mu_{xx}(y, z) &= \mu_0 h^2, & \epsilon_{xx}(y, z) &= \epsilon_0 h^2, \\ \mu_{yy}(y, z) &= \mu_0, & \epsilon_{yy}(y, z) &= \epsilon_0, \\ \mu_{zz}(y, z) &= \mu_0, & \epsilon_{zz}(y, z) &= \epsilon_0. \end{aligned} \tag{24}$$

The relationships show that the parallel-wall guide according to Fig. 1(b) filled with an anisotropic and transversely nonuniform medium is equivalent to the deformed-wall guide according to Fig. 1(a). Knowing the field distributions and properties of the former, we can compute the data of the latter structure by the use of the relationships described by (24).

We note that the properties of the medium in the parallel-wall guide are described by a tensor permeability $|\mu|$ and a tensor permittivity $|\epsilon|$ given by

$$|\mu| = \begin{vmatrix} h^2(y, z)\mu_0 & 0 & 0 \\ 0 & \mu_0 & 0 \\ 0 & 0 & \mu_0 \end{vmatrix} \tag{25}$$

and

$$|\epsilon| = \begin{vmatrix} h^2(y, z)\epsilon_0 & 0 & 0 \\ 0 & \epsilon_0 & 0 \\ 0 & 0 & \epsilon_0 \end{vmatrix}. \tag{26}$$

The equations show that the longitudinal components (with respect to the guide) of the relative material constants μ_r and ϵ_r are proportional to h^2 which is a function of the cross-sectional position. The relative material constants μ_r and ϵ_r are given by $\mu = \mu_0\mu_r$ and $\epsilon = \epsilon_0\epsilon_r$, respectively.

Let us next represent the cross-sectional coordinates for the two guides shown in Fig. 1 in complex planes [4, 5] where

$$U = v + jw, \tag{27}$$

and

$$X = y + jz. \tag{28}$$

The coordinates are interrelated by a complex function

$$U = f(X). \tag{29}$$

We postulate that U is a conformal image of X. We write

$$dU/dX = A \exp j\alpha. \tag{30}$$

Using these notations, h becomes

$$h = A = |dU/dX|. \tag{31}$$

The longitudinal relative permittivity and permeability are hence equal to the scale factor (31) of the conformal transformations of the coordinates of the two systems.

A Method for Considering the Groove Guide

The derived relationships indicate the possibility of computing the field distributions and properties of the guide with arbitrarily deformed walls as shown in Fig. 1(a) by considering a parallel-wall guide filled with an anisotropic and nonuniform medium as an intermediate step. The relationships suggest the following procedure.

First, we present the cross section of the deformed-wall guide in the complex plane and determine the complex function [4, 5] which transforms the cross section into two straight parallel lines. If the transformation function is analytic, the Cauchy-Riemann equations are satisfied, and the transformation represents a conformal mapping. The scale factor $h(y, z)$ of the conformal mapping yields the longitudinal components of the anisotropic relative permittivity and permeability [(25) and (26)] of the medium which fills the hypothetical parallel-wall guide to give equal properties. We compute next the field distribution within and the properties of the parallel-wall guide. The basic properties, such as the exponential decrease of the field intensities in direction from the center, the cutoff wavelength λ_c, the guide wavelength λ_g, etc., are independent of the transformation and the same for both guides. The magnitudes of the field intensities are interrelated by (24).

For the determination of the scale factor $h(y, z)$ and of the complex transformation function $f(X)$, mathematical procedures shown in the following section are suitable. This section shows the application of the Schwartz-Christoffel theorem [4, 5] for the rigorous computation of the transformation function. Graphical methods and experimental electrolytic-tank procedures for field mapping can be applied also; they yield directly the scale factor h without the necessity of determining the transformation function [6].

Rectangular Cross Section of the Groove

The guide with a rectangular cross section of the groove represents a typical, practical example of the new guide. This particular cross section is interesting since the transformation function and the scale factor can be determined rigorously by conformal mapping. The cross section of the guide has the form and the dimensions shown in Fig. 2. The total height of the guide is h, and the distance between the parallel walls is p. The width and depth of the rectangular grooves are Δh and Δp, respectively. The cross section as shown in Fig. 2, plotted in the complex plane, can be transformed by a complex function into two straight parallel lines. The Schwartz-Christoffel theorem is applied for finding this function [4, 5].

Since the cross section of the guide is symmetrical, we consider one quadrant only and place it on the complex U plane with v and w as coordinates. The conditions are indicated in Fig. 3(a). The contour of the quadrant of the guide with infinite walls follows the lines from 0 to A, B, C, D, E, and back to 0. The point D is at infinity. This contour has to be transformed into a rectangle, as shown in Fig. 3(c). The transformed cross section is plotted in the complex X plane where $X=y+jz$.

For simplifying the transformation procedure, a complex T plane is introduced as an intermediate step [Fig. 3(b)]. The coordinates are r and s; the complex function becomes $T=r+js$. This assumption allows mapping the complex T plane onto the U and X planes. Elimination of T yields the transformation function between U and X. In the T plane, the contour representing the considered quadrant of the guide is found on the real axis with the images of the points 0 and A to E denoted by the same letters. The connecting line between the points D in the T plane is a circle with infinite radius.

Using the Schwartz-Christoffel theorem, we find for the transformations the following relations:

$$dU/dT = K_1(T - r_2)^{1/2}(T^2 - 1)^{-1/2}(T - r_1)^{-1/2}, \quad (32)$$

$$dX/dT = K_2(T + 1)^{-1/2}(T - 1)^{-1/2}, \quad (33)$$

$$dU/dX = (T - r_2)^{1/2}(T - r_1)^{-1/2}. \quad (34)$$

Evaluation of (33) yields

$$T = -\cos(2\pi X/p + \pi/2). \quad (35)$$

Substitution in (34) and integration gives the transformation function from

$$dU/dX = (\sin 2\pi X/p + r_2)^{1/2}(\sin 2\pi X/p + r_1)^{-1/2}. \quad (36)$$

The scale factor is obtained from (34). It becomes, after separating X in real and imaginary parts,

$$h^2 = \left[\frac{(\cos\phi\cosh\psi + r_2)^2 + (\sin\phi\sinh\psi)^2}{(\cos\phi\cosh\psi + r_1)^2 + (\sin\phi\sinh\psi)^2}\right]^{\frac{1}{2}}, \quad (37)$$

where $\phi = 2\pi y/p + \pi/2$ and $\Psi = 2\pi z/p$.

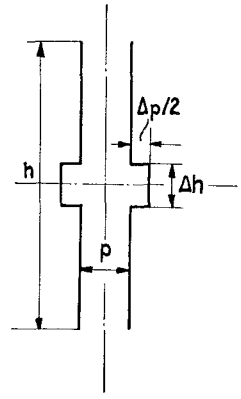

Fig. 2—Cross section of the rectangular-groove guide.

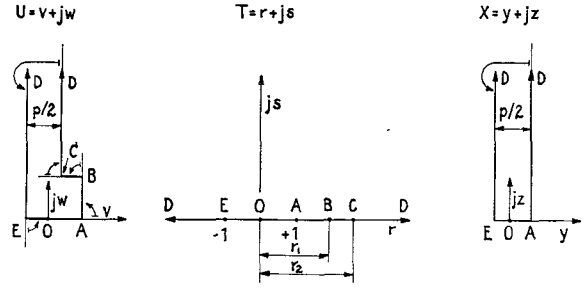

Fig. 3—Quadrant of guide cross section before and after transformation in the complex plane. (a) Original cross section. (b) and (c) Cross sections after transformation.

The determination of the constants r_2 and r_1 is rather tedious and is omitted here. It should be noted that the computation leads to elliptical integrals for which tables can be found in Byrd and Friedman [7]. A plot of the constants r_2 and r_1 versus $\Delta p/p$ and $\Delta h/p$ is shown in Fig. 4. With the constants known, we can find h^2 and consequently the components of the relative permittivity and permeability according to (25) and (26). Fig. 5 shows an example of a typical distribution of these material constants in the yz-plane where the density of shading represents a measure of their magnitude.

We observe that the medium constants are increased in the central region of the cross section above the free space value which is 1. The increase becomes considerable near the images of the points A and B, which denote the bottom of the groove. A decrease of the constants occurs near the image of the corner point C which is located at the rim of the rectangular groove [Fig. 3(a)].

The next step in considering the groove guide consists in the computation of the field distribution within the guide with the cross section shown in Fig. 1(b) filled with a medium with medium constants given by h^2 with a distribution as indicated in Fig. 5. Methods for the computation of electromagnetic fields in nonumiform media can be used for this purpose. Procedures are described in the literature (Schelkunoff [4], Collin [9] and Tischer [8]. A special treatment of this problem is in

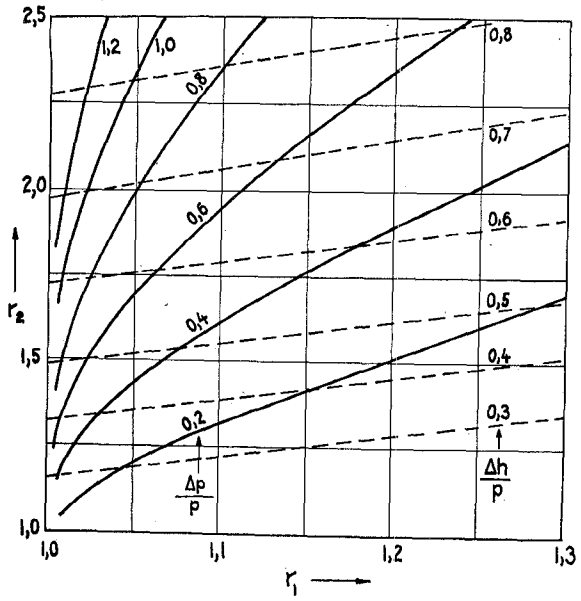

Fig. 4—Constants r_2 and r_1 (38) vs relative groove width $\Delta h/p$ and depth $\Delta p/p$.

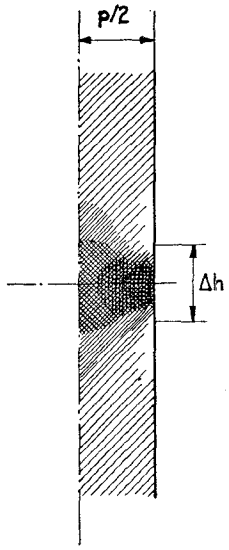

Fig. 5—Typical distribution of the relative permittivity and permeability [(25) and (26)] of the medium in the parallel-wall guide.

preparation. Knowing the field distribution, we can compute the general data of a parallel-wall guide and apply the results to the groove guide.

An alternative, simplified method for estimates of the cutoff and guide wavelengths applying the results of computations of the data of the H-guide is shown in the next section.

A Rough Estimate of the Cutoff and Guide Wavelengths

We can obtain a rough estimate of the cutoff and guide wavelengths of the rectangular groove guide without carrying out the computation of the field distribution by using the results of the following approximate consideration. We substitute for the central section of the air-filled guide which includes the two

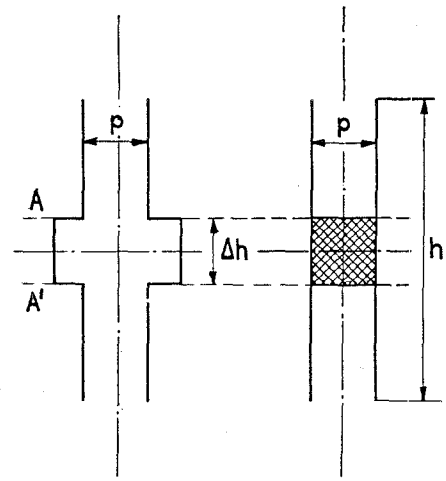

Fig. 6—Replacement of the central guide section by a dielectric-filled section.

rectangular grooves a dielectric-filled section of a width equal to that of the rest of the guide. The relative permittivity of the substituted section is chosen uniform and has such a value that the cutoff and guide wavelengths equal those of the air-filled section which includes the grooves. Fig. 6 shows, on the right-hand side, the substituted section filled with the uniform and isotropic dielectric.

For finding the relative permittivity of the dielectric, we have to equate the cutoff wavelengths of both guide sections between A and A' as indicated in Fig. 6. We find

$$\lambda_c^2 = [2(p + \Delta p)]^2 = \epsilon_r(2p)^2, \tag{38}$$

which yields

$$\epsilon_r = (1 + \Delta p/p)^2,$$

and

$$\epsilon_r \approx 1 + 2\Delta p/p, \tag{39}$$

if Δp is a fraction of the width $p(\Delta p \ll p)$. Knowing the permittivity of the dielectric slab, we use relations derived for the cutoff and guide wavelengths of the H-guide for the determination of these quantities of the groove guide. The relations involved are [1, 2]

$$k_a^2 + k_d = (\epsilon_r - 1)(2\pi/\lambda_0)^2, \tag{40}$$

$$\tan (k_d \Delta h/2) = \epsilon_r k_a/k_d, \tag{41}$$

$$k_a^2 = (2\pi/\lambda_g)^2 - (2\pi/\lambda_0)^2 + (\pi/p)^2, \tag{42}$$

where k_a and k_d are constants, λ_0 is the same free-space wavelength corresponding to the frequency of the transmitted signals, and λ_g is the wavelength within the guide. The cutoff wavelength λ_c is given by

$$(1/\lambda_c)^2 = (1/\lambda_0)^2 - (1/\lambda_g)^2. \tag{43}$$

Evaluation of (40) to (43), usually performed graphically, yields λ_c and λ_g which is the same for both guides. It should be noted that the constant k_d represents the constant for the exponential decrease of the field intensities in direction parallel to the walls and in direc-

tion from the centrally-located dielectric slab. The value of k_d is approximately the same in the case of the groove guide.

Conclusion

It is shown that a deformed-wall guide with grooves in the central region of the cross section is equivalent to a parallel-wall guide with a dielectric contained in the central section. The guide has, consequently, similar properties to those of an H-guide. Theoretically, it is characterized by low attenuation which decreases with increasing frequency and by an exponentially decreasing field distribution in the direction from the center of the cross section parallel to the walls. Since the guide contains no dielectric, it is expected to have a lower attenuation than the H-guide. Besides the application for long-distance transmission and as a delay line, the simple structure makes the guide suitable for the design of millimeter wave circuitry and of circuit elements.

References

[1] F. J. Tischer, "A waveguide with low losses," *Arch. der Elektr. Uebertragung*, vol. 7, pp. 592–596; 1953.
[2] F. J. Tischer, "The H-guide, a waveguide for microwaves," 1956 IRE Convention Record, pt. 5, pp. 44–51.
[3] J. A. Stratton, "Electromagnetic Theory," McGraw-Hill Book Co., Inc., New York, N. Y.; 1941.
[4] S. A. Schelkunoff, "Applied Mathematics for Engineers and Scientists," D. Van Nostrand Co., Inc., Princeton, N. J.; 1948.
[5] L. Bieberbach, "Conformal Mapping," Chelsea Publishing Co., New York, N. Y.; 1953.
[6] S. Ramo and J. R. Whinnery, "Fields and Waves in Modern Radio," John Wiley & Sons, Inc., New York, N. Y.; 1953.
[7] P. F. Byrd and M. D. Friedman, "Handbook of Elliptic Integrals for Engineers and Physicists," Springer Verlag, Berlin, Germany; 1954.
[8] F. J. Tischer, "Propagation-Doppler effects in space communications," Proc. IRE, vol. 48, pp. 570–574; April, 1960.
[9] R. E. Collin, "Field Theory of Guided Waves," McGraw-Hill Book Co., Inc., New York, N. Y.; 1960.

Factors Affecting Earth-Satellite Millimeter Wavelength Communications*

A. W. STRAITON†, fellow, ieee, and C. W. TOLBERT†, senior member, ieee

Summary—**The use of millimeter wavelengths for earth-satellite transmissions is suggested by the large bandwidths and high gain with small antennas possible at these wavelengths. The factors discussed are 1) propagation path loss, 2) refraction, and 3) antenna temperature.**

The attenuation through the entire atmosphere over the millimeter spectrum is given as a function of elevation angle of the antenna beam. The attenuation and scattering loss due to water and ice particles varies over a wide range of values depending on the number of particles and their sizes.

Refraction by the atmosphere is less than one milliradian for elevation angles for which the absorption is low enough to make the transmission practical. Fluctuations due to refraction may, however, be quite severe.

Contribution to antenna temperatures from the atmosphere, the earth, the sun and moon are given for earth-based antennas and antennas in space.

Introduction

EARTH-SATELLITE millimeter wavelength applications, as the name implies, involve transmission through the earth's atmosphere. It is the purpose of this paper to discuss several of the important factors which determine the propagation characteristics of wavelengths from 1 mm to 1 cm and to present the results of recent measurements which provide further quantitative evaluations of these factors.

* Received January 21, 1963; revised manuscript received June 3, 1963. The data presented in this paper was obtained under Air Force Contracts No. 19(604)-8036 and No. AF 33(657)-7333.

† Electrical Engineering Research Laboratory, The University of Texas, Austin, Tex.

This paper will be concerned with 1) propagation path loss, 2) refraction, and 3) antenna temperature. These factors are pertinent to both active and passive systems, and form the framework for the choice or rejection of a millimeter wavelength for a particular application.

Propagation Path Losses

The losses experienced in propagating millimeter wavelengths through the earth's atmosphere, other than free-space losses, are caused predominantly by atmospheric gases, clouds, particles and precipitation. Longer wavelengths are attenuated by the same mechanisms but to a lesser degree because of the remoteness of the wavelengths from the resonant frequency of the gas and the smaller size of precipitation and cloud particles relative to the longer wavelengths.

The attenuation by atmospheric gases is primarily associated with oxygen and water vapor molecules and is most conveniently described by the Van Vleck-Weisskopf equation.[1] Due to the magnetic moments associated with oxygen and the electric moments associated with water vapor, there are a large number of energy transitions that produce peak values of absorption at millimeter wavelengths. Most of the energy transi-

[1] J. H. Van Vleck and V. F. Weisskopf, "On the shape of collision broadened lines," *Rev. Mod. Phys.*, vol. 17, pp. 227–236; April–July, 1945.